

Origin of the variation in lattice thermal conductivities in pyrite-type dichalcogenides

Tiantian Jia ¹, Xiaobing Liu,² Yongsheng Zhang ^{2,*} and Su-Huai Wei ^{1,†}

¹Beijing Computational Science Research Center, Beijing 100193, China

²Advanced Research Institute of Multidisciplinary Sciences, Qufu Normal University, Qufu 273165, China



(Received 3 October 2022; revised 22 February 2023; accepted 1 March 2023; published 17 March 2023)

Lattice thermal conductivity is a crucial parameter for thermoelectric (TE) applications. In pyrite-type metal dichalcogenides, it is observed that the type of metal atom has a significant influence in the phonon properties and lattice thermal conductivities, but the physical origin is not clear. In this paper, we show that, for the pyrite-type posttransition metal (such as Zn or Cd) dichalcogenides, because the fully occupied d^{10} orbitals inside the valence bands are relatively localized, the enhanced symmetry-controlled s - d coupling effects in the posttransition metal atoms when they vibrate away from the high-symmetry equilibrium positions can lead to soft phonon properties and strong anharmonicity. Thus, they behave as rattlinglike atoms, and these systems have extremely low lattice thermal conductivities. However, for some pyrite-type transition metal dichalcogenides, when the outermost d electrons in transition metal atoms are only occupied by the T_{2g} -derived states, such as Fe with d^6 configuration, the symmetry-controlled s - d coupling effects in the transition metal atoms are strongly cancelled by the varying crystal field splitting when symmetry is reduced during vibration. Therefore, these compounds exhibit hard phonon properties, weak anharmonicities, and high lattice thermal conductivities. In this paper, we reveal the electronic origin of the puzzling behaviors of pyrite-type dichalcogenides which show a wide range of thermal conductivity properties. The discussed mechanism can also be used to guide researchers in seeking promising TE materials with low lattice thermal conductivity.

DOI: [10.1103/PhysRevB.107.115204](https://doi.org/10.1103/PhysRevB.107.115204)

I. INTRODUCTION

The conversion efficiency of the thermoelectric (TE) device depends on the dimensionless TE figure of merit $ZT = S^2\sigma T/\kappa$, where T is the absolute temperature, S is the Seebeck coefficient, σ is the electrical conductivity, and κ is the thermal conductivity including carrier (κ_e) and lattice (κ_l) contributions. The promising TE materials need a high power factor ($PF = S^2\sigma$) and low κ_l . According to the Boltzmann transport theory [1], S , σ , and κ_e are determined by the electrical transport properties, while κ_l is mainly contributed by the phonon properties. Due to the competition between these electrical parameters (S , σ , and κ_e), the practical TE materials are almost invariably semiconductors. For most semiconductors, κ is mainly contributed by κ_l . Seeking the semiconductors with low κ_l is crucial for TE, which enables us to simplify complex TE parameters and focus on optimizing electrical transport properties. Therefore, uncovering the fundamental physical mechanisms of low κ_l is significant for seeking and designing high-performance TE materials.

It is well known that low κ_l arises from strong phonon scatterings and short phonon lifetimes. In a solid, for the acoustic phonons, the normal phonon scatterings and Umklapp phonon-phonon scatterings are both proportional to the square of anharmonicity [Grüneisen parameter (γ)] and negatively correlated with the sound speed (v) [2–4]. According to previous works [5–7], the lattice thermal conductivity ap-

proximately satisfies $\kappa_l \propto \frac{v^3}{\gamma^2}$. This means that the slow sound speed (soft phonon properties) and strong anharmonicity can result in low lattice thermal conductivity. Under the acoustic approximation of elastic waves, the sound speed (v) is decided by the atomic mass (m) and bond strength (the spring constant k), as $v \sim \sqrt{k/m}$ [8]. This shows that the atoms with weak chemical bonds and heavy atomic masses can exhibit slow sound speed and soft phonon properties. Exploring the unique characteristics of chemical bonds in different materials can help us to better understand the physical mechanisms of low κ_l . Anharmonicity is the deviation of a balanced system from a harmonic oscillator, which can be measured by the change of the potential energy with the atomic displacement. Since the potential energy is decided by the atomic configurations in a solid, many previous researchers have reported that some unique bonding characteristics (such as lone pair electrons [9,10], resonant bondings [7,11], and rattling models [12–17], etc. [18]) can contribute to the strong anharmonicities in high-performance TE materials. However, the common fundamental mechanisms behind these characteristics remain elusive. In recent years, it was found [19–21] that the symmetry-controlled s - d coupling effect caused by the coupling of occupied d electrons and unoccupied s electrons in Cu atoms plays a critical role in determining the distinct diffusion behaviors of Cu atoms in semiconductors and the anomalous ground-state structures of Cu-based materials. This means that the electronic coupling between occupied and unoccupied states contributes significantly to the potential energy surfaces and vibrational properties of atoms in a system. By comparing the atomic orbital couplings before and after the atomic displacement, Yang *et al.* [22] have revealed that

*yshzhang@qfnu.edu.cn

†suhuaiwei@csrc.ac.cn

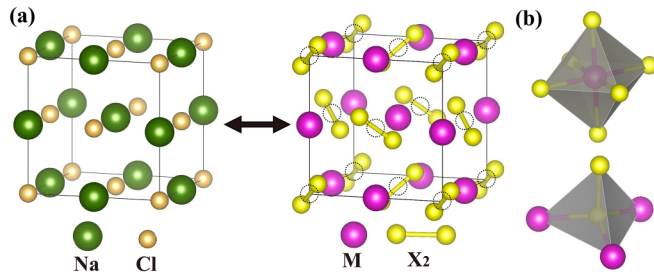


FIG. 1. (a) Crystal structure comparison between the rock-salt structure (left) and the pyrite-type dichalcogenides (MX_2 , right). The empty circles in the left panel represent the center of the dimer. (b) The bonding configurations of the different atoms in the pyrite-type dichalcogenides.

the fundamental origin of the strong anharmonicity observed in the Cu-based materials is the strong symmetry-controlled s - d coupling effect, which occurs when Cu atoms vibrate away from equilibrium positions. Their work offered insight at the atomic level connecting electronic structures with phonon vibration modes, which can be used to explore the fundamental mechanisms of strong anharmonicities in other materials.

The pyrite-type dichalcogenides are the transition or posttransition metal dichalcogenides (MX_2 , where M is transition or posttransition metal; $X = S, Se, \text{ or } Te$) and share the same space group ($Pa\bar{3}$) with FeS_2 (pyrite), which adopts a NaCl-like face-centered cubic structure with the center of X - X nonmetallic dimers occupying the anion positions, as shown in Fig. 1(a). In the structure, the M atom is located at the center of an octahedron with six X atoms at the vertexes, and each X atom sits at the center of a tetrahedron and is bonded with three M atoms and one X atom, as shown in Fig. 1(b). The pyrite-type dichalcogenides are a large family of compounds, which include the known minerals and the high-pressure synthesized compounds: FeX_2 , MnX_2 , CoX_2 , NiX_2 , CuX_2 , ZnX_2 , and CdX_2 [23]. Due to the high-symmetry cubic structure and ideal electronic band structures (possessing multiple carrier pockets with optimal effective masses near the Fermi level), many pyrite-type dichalcogenides have been reported to possess the promising electrical transport properties and good TE properties, such as FeX_2 [24–26], $MnTe_2$ [27], $RuSe_2$ [28], and NiS_2 [29]. However, some experimental studies have shown that many common pyrite-type dichalcogenides have high thermal conductivities (e.g., the experimental thermal conductivities at room temperature are ~ 47.8 and 10.8 W/mK for single-crystalline FeS_2 [30] and polycrystalline CoS_2 [31], respectively), which limits the application and development of these common pyrite-type dichalcogenides in the field of TE.

Recently, using knowledge-based high-throughput material searches [32] and detailed theoretical calculations [16,17], we have predicted that four pyrite-type IIB-VIA₂ dichalcogenides (ZnS_2 , $ZnSe_2$, CdS_2 , and $CdSe_2$) with rattlinglike metal atoms and strong nonmetallic dimers possess good electrical transport properties and low lattice thermal conductivities. One of the curious questions is why different pyrite-type dichalcogenides with the same crystal structure and similar nonmetallic dimers (X - X) have such markedly different thermal conductivities. In this paper, to better understand the physical mechanisms

behind it, we analyze and compare phonon vibrational properties, chemical bonding situations, and atomic orbital couplings of six different pyrite-type dichalcogenides (ZnS_2 , CdS_2 , FeS_2 , $ZnSe_2$, $CdSe_2$, and $FeSe_2$) and explore the intrinsic origin of the variation in lattice thermal conductivities in pyrite-type dichalcogenides. We reveal that the posttransition metal atoms with the fully occupied and chemically inert localized d electrons can behave as rattlinglike atoms, and the enhancement of the symmetry-controlled s - d coupling effects in the posttransition metal atoms with the reduction of the crystal field symmetry can contribute to the soft phonon properties and strong anharmonicities of the corresponding pyrite-type dichalcogenides. However, the partially occupied d electrons involved in chemical bonding and the crystal field splitting of the d orbitals in the transition metal atoms sensitive to the change of the crystal symmetry are responsible for the strong chemical bonds (hard phonon properties), weak anharmonicities, and high lattice thermal conductivities of the corresponding pyrite-type dichalcogenides. In this paper, we suggest that the pyrite-type dichalcogenides formed by the posttransition metal atoms with both fully occupied localized d electrons and strong symmetry-controlled s - d coupling effects can exhibit low lattice thermal conductivities.

II. COMPUTATIONAL METHODOLOGIES

In this paper, density functional theory (DFT) as implemented in the Vienna *Ab initio* Simulation Package [33] code with the projector augmented-wave method [34] is used to calculate the structural parameters and electronic properties of different pyrite-type dichalcogenides. The generalized gradient approximation in the scheme of Perdew-Burke-Ernzerhof (PBE) [35] is carried out to account for the electronic exchange and correlation energy of Zn- and Cd-based dichalcogenides. Our previous studies [16,17] have shown that the PBE calculations are satisfactory for the corresponding systems, e.g., the calculated lattice constants are in good agreement with the experimental measurements for Zn- and Cd-based dichalcogenides. The Hubbard U correction [36] (PBE+ U) is adopted for better treatment of Fe-based dichalcogenides, and the effective U of 2 eV is chosen for Fe 3d orbitals, which had been shown to give a more correct description on the electronic properties of pyrite FeS_2 [37]. The energy cutoff for the plane-wave expansion is set to 420 eV. All geometry structures are relaxed until the convergence of the total energies are $< 10^{-5}$ eV and the force on each atom is < 0.01 eV/Å. The Brillouin zone is sampled using the Monkhorst-Pack method [38] with the special k-points of a $7 \times 7 \times 7$ grid for the geometry optimizations and a $35 \times 35 \times 35$ grid for the electronic density of states (DOS) calculations. In this paper, the PBE+ U optimized lattice constants of FeS_2 and $FeSe_2$ are 5.4265 and 5.8054 Å, which are in reasonable agreement with experimental measurements (5.4182 and 5.7859 Å) [23], and the calculated band gaps are 1.04 and 0.54 eV [as shown in Fig. 2(a)], which are close to the previous theoretical results (1.03 and 0.69 eV for FeS_2 [39] and $FeSe_2$ [26], respectively). Furthermore, because the hybrid functional proposed by Heyd, Scuseria, and Ernzerhof (HSE06) [40,41] has been demonstrated to be a more

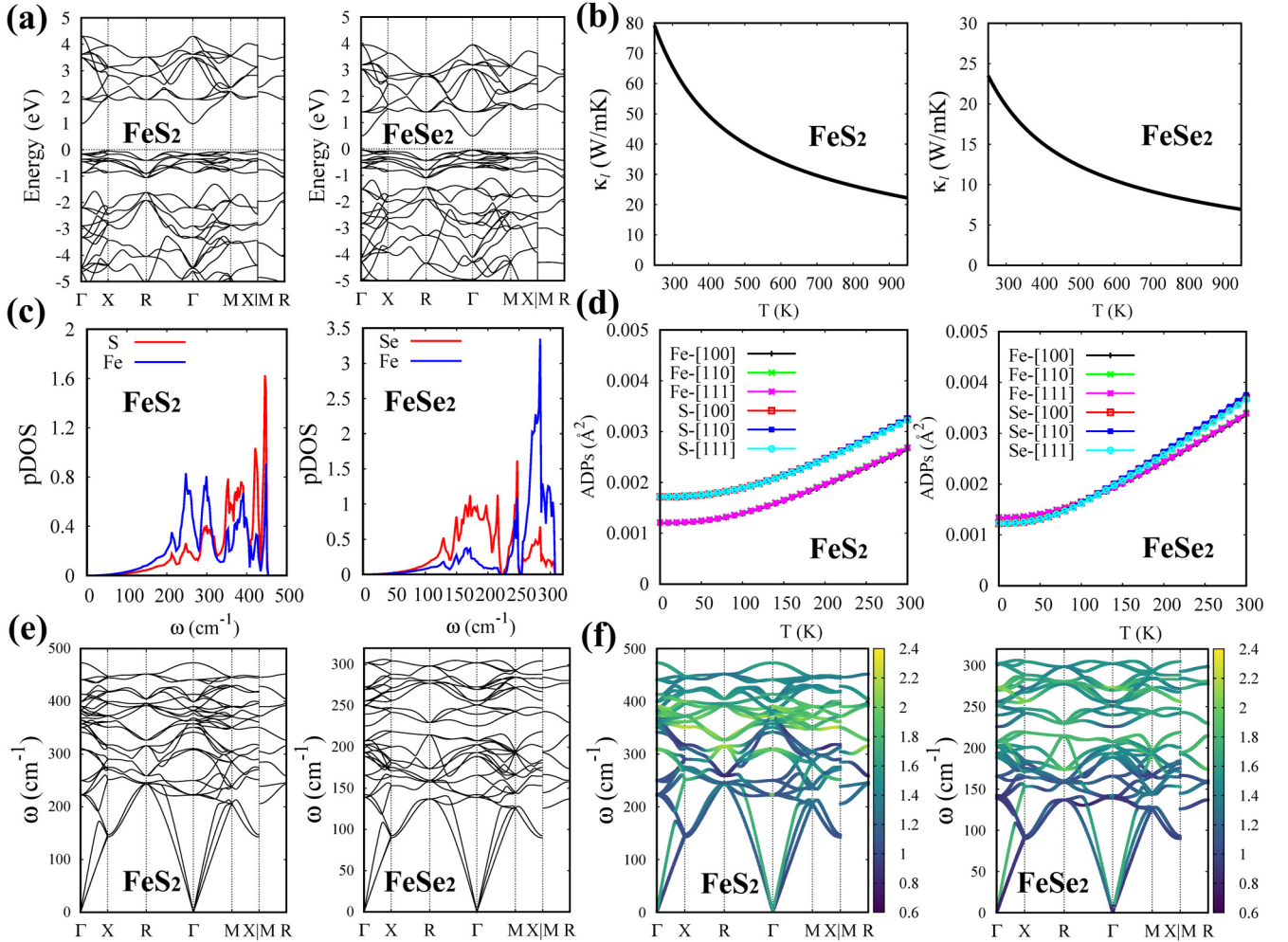


FIG. 2. (a) Calculated electronic band structures, (b) lattice thermal conductivities (κ_l), (c) phonon densities of states (pDOS), (d) atomic displacement parameters (ADPs), (e) phonon dispersions, and (f) Grüneisen parameters (γ) in FeS₂ and FeSe₂.

reliable method to calculate the structural, electronic, and defect properties in semiconductors [42,43], to further evaluate the reliability of the computational methods used in this paper, we calculate and compare the electronic band structures and the total potential energy curves as a function of the displacements of the metal atoms vibrated away from the equilibrium positions along the [111] direction in three pyrite-type dichalcogenides (ZnS₂, CdS₂, and FeS₂) using the different computational methods (PBE, PBE+ U under different U values, and HSE), as shown in Figs. S1–S3 in the Supplemental Material [44]. We find that the different computational methods have little effect on the band features and the lattice vibrational potential energy of the same compound. This indicates that, for the studied systems, it is reasonable to use PBE and PBE+ U methods to describe the electronic and phonon properties of the different pyrite-type dichalcogenides.

The phonon vibrational properties of different pyrite-type dichalcogenides are calculated using the finite displacement method as implemented in the PHONOPY software package [45]. To obtain reliable phonon dispersions, the geometric structures are further optimized until the convergence of the total energies is $<10^{-8}$ eV and the force on each atom is

$<10^{-4}$ eV/Å with a more refined $8 \times 8 \times 8$ Monkhorst-Pack k-points sampling. The $2 \times 2 \times 2$ supercells (96 atoms) are used for the second-order interatomic force constants (IFCs) calculations. The anharmonicities and the strain dependence of phonon frequencies are evaluated using Grüneisen parameters as $\gamma_i = -\frac{V}{\omega_i} \frac{\partial \omega_i}{\partial V}$ by isotropically expanding the system volume by $\pm 3\%$ from the DFT relaxed volume. The lattice thermal conductivities are calculated by solving the full linearized phonon Boltzmann transport equations (BTEs) as implemented in the ALMABTE code [46]. The Born effective charges and the dielectric tensors are evaluated from DFT calculations. The third-order IFCs are computed by resolving the irreducible set of atomic displacements from the THIR-DORDER.PY code [47]. The interatomic interactions up to the fifth coordination shell and the $7 \times 7 \times 7$ Γ -centered grids are used to solve the phonon BTEs.

III. RESULTS AND DISCUSSION

A. Lattice thermal conductivities

In our previous studies [16,17], by solving the phonon BTEs, the lattice thermal conductivities (κ_l) of four

pyrite-type Zn- and Cd-based dichalcogenides (ZnS_2 , ZnSe_2 , CdS_2 , and CdSe_2) have been calculated, and the calculated results have shown that the four compounds all have ultralow lattice thermal conductivities ($\kappa_l < 2$ W/mK at room temperature). By analyzing their phonon vibrational properties, this is attributed to the existence of rattlinglike metal atoms around the localized nonmetallic dimers [16,17]. However, by applying the same calculation method, we find that, for Fe-based dichalcogenides (FeS_2 and FeSe_2) with similar nonmetallic dimers (S-S and Se-Se), their calculated κ_l are very high [as shown in Fig. 2(b)], e.g., at 300 K, the calculated κ_l of FeS_2 is 65.8 W/mK, which shows reasonably good agreement with the experiment result (47.8 ± 2.4 W/mK) [30], and the calculated κ_l of FeSe_2 is also relatively large (19.7 W/mK at 300 K).

To analyze the origin of the significantly different lattice thermal conductivities within the pyrite-type dichalcogenides, we calculate the phonon DOS (pDOS) and atomic displacement parameters (ADPs) of each atom in Fe-based dichalcogenides (FeS_2 and FeSe_2), as shown in Figs. 2(c) and 2(d), respectively, and compare them with the corresponding Zn- and Cd-based dichalcogenides (ZnS_2 , ZnSe_2 , CdS_2 , and CdSe_2) with low lattice thermal conductivities [16,17]. In Zn- and Cd-based dichalcogenides, the localized isolated high-frequency optical phonons are completely contributed by the nonmetal atoms [16,17]. However, in Fe-based dichalcogenides, the high-frequency optical phonons are contributed by both metal and nonmetal atoms, as shown in Fig. 2(c). By comparing the bond lengths within the X - X dimers (L_{X-X}) in different pyrite-type dichalcogenides, we find that the measured L_{S-S} 's are 2.079, 2.086, and 2.145 Å for ZnS_2 , CdS_2 , and FeS_2 , respectively, and the measured L_{Se-Se} 's are 2.396, 2.397, and 2.464 Å for ZnSe_2 , CdSe_2 , and FeSe_2 , respectively. The measured L_{X-X} 's in Fe-based dichalcogenides (2.145 and 2.464 Å) are much longer than that in Zn- and Cd-based dichalcogenides, which means that the nonmetallic dimers in Fe-based dichalcogenides are weak. From Fig. 2(d), we find that the calculated ADPs of Fe atoms along different directions at 300 K are ~ 0.0027 and 0.0034 Å² in FeS_2 and FeSe_2 , respectively, which are much less than those of metal atoms in Zn- and Cd-based dichalcogenides (~ 0.015 – 0.025 Å²) [16,17]. This means that Fe atoms in Fe-based dichalcogenides do not move easily and cannot exhibit rattlinglike vibration properties. Furthermore, we calculate the phonon dispersions [as shown in Fig. 2(e)] and anharmonicity parameters [Grüneisen parameters (γ), as shown in Fig. 2(f)] in FeS_2 and FeSe_2 . We find that their average acoustic phonon frequencies and lowest optical phonon frequencies (ω_a^{av} , ω_o^{min}) are (165.5, 151.5) and (101.2, 95.4) cm⁻¹, respectively, which are much larger than those in Zn- and Cd-based dichalcogenides (ω_a^{av} 's are 63.9, 45.7, 44.6, and 33.0 cm⁻¹, and ω_o^{min} 's are 69.0, 49.2, 45.8, and 33.9 cm⁻¹ for ZnS_2 , ZnSe_2 , CdS_2 , and CdSe_2 , respectively). Their maximum Grüneisen parameters in acoustic phonons (γ_a^{max}) and in low-frequency optical phonons (with the frequency smaller than $2\omega_o^{\text{min}}$, γ_o^{max}) are (1.80, 2.01) and (1.82, 1.96), respectively, which are much less than those in Zn- and Cd-based dichalcogenides (γ_a^{max} 's are 4.60, 4.60, 3.18, and 2.72, and γ_o^{max} 's are 3.55, 3.76, 2.43, and 2.47 for ZnS_2 , ZnSe_2 , CdS_2 , and CdSe_2 , respectively). These data are listed in Table I. This means that, although

TABLE I. Calculated lattice thermal conductivities at 300 K (κ_l), average acoustic phonon frequencies (ω_a^{av}), lowest optical phonon frequencies (ω_o^{min}), maximum Grüneisen parameters in acoustic phonons (γ_a^{max}), and maximum Grüneisen parameters in low-frequency optical phonons with the frequency smaller than $2\omega_o^{\text{min}}$ (γ_o^{max}) in ZnS_2 , ZnSe_2 , CdS_2 , CdSe_2 , FeS_2 , and FeSe_2 .

MX_2	ZnS_2	ZnSe_2	CdS_2	CdSe_2	FeS_2	FeSe_2
κ_l (W/mK)	1.55	0.69	1.47	0.75	65.8	19.7
ω_a^{av} (cm ⁻¹)	63.9	45.7	44.6	33.0	165.5	101.2
ω_o^{min} (cm ⁻¹)	69.0	49.2	45.8	33.9	151.5	95.4
γ_a^{max}	4.60	4.60	3.18	2.72	1.80	1.82
γ_o^{max}	3.55	3.76	2.43	2.47	2.01	1.96

the nonmetallic dimers exist in the pyrite-type Fe-based dichalcogenides (FeS_2 and FeSe_2), they can neither possess rattlinglike metal atoms nor the soft phonon modes and strong anharmonicities, which will result in possible high lattice thermal conductivities. Therefore, it is useful to further explore the fundamental mechanisms of the soft phonon modes and strong anharmonicities from the atomic level in the pyrite-type Zn- and Cd-based dichalcogenides.

B. Soft phonon modes

Our previous studies have shown that the soft phonon modes are mainly contributed by rattlinglike metal atoms in the pyrite-type Zn- and Cd-based dichalcogenides [16,17]. Since the chemical bond plays an important role in determining the phonon properties, to explore the intrinsic origin and fundamental physical mechanism of the soft phonon modes in Zn- and Cd-based dichalcogenides, we further analyze and compare the bonding characteristics of the different metal atoms in these pyrite-type dichalcogenides.

Figure 3 shows the electron projected DOS (ePDOS) of six different pyrite-type dichalcogenides (ZnS_2 , CdS_2 , FeS_2 , ZnSe_2 , CdSe_2 , and FeSe_2). For Zn- and Cd-based dichalcogenides, due to the similar valence electron configurations in Zn and Cd atoms, $3d^{10}4s^2$ and $4d^{10}5s^2$, respectively, the outermost Zn_{3d} and Cd_{4d} orbitals are fully occupied. From the calculated ePDOS in Figs. 3(a)/3(b) and 3(d)/3(e), $\text{Zn}_{3d}/\text{Cd}_{4d}$ states in Zn-/Cd-based dichalcogenides are located inside the valence band. The top of the valence bands is mainly composed of $\text{S}_{3p}/\text{Se}_{4p}$ states with a small amount of metal d characters, and the bottom of the conduction bands is mainly constituted by $\text{Zn}_{4s}/\text{Cd}_{5s}$ and $\text{S}_{3p}/\text{Se}_{4p}$ states together. This means that the chemical bonds in Zn-/Cd-based dichalcogenides are mainly formed by $\text{Zn}_{4s}/\text{Cd}_{5s}$ and $\text{S}_{3p}/\text{Se}_{4p}$ electrons. However, for Fe-based dichalcogenides, since the valence electron configuration in Fe atoms is $3d^64s^2$ and the outermost Fe_{3d} orbitals are partly occupied and more chemically active, the Fe_{3d} states are distributed in a large energy range [as shown in Figs. 3(c)/3(f), the couplings between Fe_{3d} and $\text{S}_{3p}/\text{Se}_{4p}$ states dominate the top of the valence bands and the bottom of the conduction bands]. Therefore, unlike the chemical bonds formed by M- s and S/Se- p electrons in Zn-/Cd-based dichalcogenides, the chemical bonds in Fe-based dichalcogenides are mainly formed by Fe- $3d$ and S/Se- p electrons. The strengths of chemical bonds in

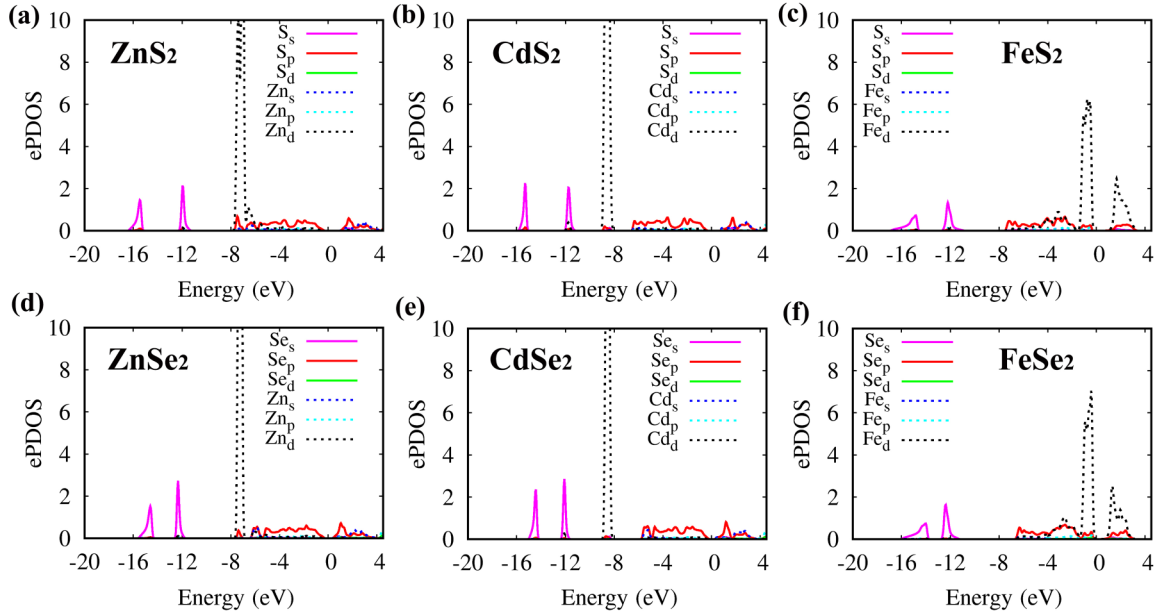


FIG. 3. Calculated electron projected densities of states (ePDOS) in (a) ZnS₂, (b) CdS₂, (c) FeS₂, (d) ZnSe₂, (e) CdSe₂, and (f) FeSe₂.

Fe-based dichalcogenides are stronger than those in Zn-/Cd-based dichalcogenides due to coupling to the unoccupied d electrons in Fe atoms. The weaker chemical bonds in Zn-/Cd-based dichalcogenides leads to soft phonon properties compared with those of Fe-based dichalcogenides. Therefore, we infer that the metal atoms with the fully occupied and chemically inert low-binding-energy d electrons (such as Zn or Cd) can behave as rattlinglike atoms and exhibit soft phonon modes in pyrite-type dichalcogenides.

C. Strong anharmonicities

In classical mechanics, the anharmonicity is the deviation of a system from being a harmonic oscillator, which can be quantified by the deviation of potential energy from the harmonic one. Usually, the slower the increase of the potential energy with the atomic displacement, the larger the anharmonicity is in the system [22]. In a semiconductor, when atoms vibrate away from the equilibrium positions, in addition to the increase of the potential energy due to the change of Coulomb interactions and strain energy, the potential energy also can be affected by the change of coupling between different electronic states upon symmetry change. For example, the strong symmetry-controlled s - d coupling effects in Cu atoms can decrease the occupied d -orbital energies and increase the unoccupied s -orbital energy, which has been used to successfully explain the fundamental mechanisms of strong anharmonicities in Cu-based compounds [22] and distinct diffusion behaviors of Cu atoms in semiconductors [20].

Our previous studies have shown that the strong anharmonicities of the low-frequency optical phonons in ZnSe₂ are mainly contributed by the vibrations of Zn atoms [11]. This indicates that the metal atoms bonded with the neighboring nonmetal atoms in Zn-based dichalcogenides can possess an anharmonic behavior. To reveal the intrinsic origin and fun-

damental physical mechanism of the strong anharmonicities, we analyze the electronic coupling configurations in the metal atoms before and after the metal atoms vibrate away from the equilibrium positions. In the pyrite-type systems, the metal atom prefers to exhibit the +II oxidation state (M^{2+}), and the equilibrium position of the metal atom is located at the center of a nearly regular octahedron and the corresponding site symmetry is S_6 , which is a subgroup of O_h . Under such site symmetry, the occupied d orbitals are split by crystal field, and the corresponding symmetry of d orbitals is reduced to three parts: one A_g and one E_g state, which are derived from the T_{2g} state, and another E_g state. Meanwhile, the symmetry of the unoccupied s orbital is A_g , which will exhibit a weak s - d coupling with the d - A_g orbital due to the same symmetry. However, when the metal atoms vibrate away from the equilibrium positions, the corresponding site symmetry is further reduced to C_1 . In this case, the symmetry of the s orbital is reduced to A , and the symmetry of d orbitals is reduced to $5A$. As a result, the symmetry-controlled s - d coupling effects are enhanced, which give rise to the decrement of the occupied d -orbital energies and the increment of the unoccupied s -orbital energy; thus, the electronic energy of the system is lowered. By taking the Zn atom with the fully occupied d electrons as an example, the crystal field-induced splitting of the d orbitals and the symmetry-controlled s - d coupling effects in metal ion (M^{2+} : Zn²⁺) under different crystal symmetries are shown in Fig. 4(a).

To check this analysis, we shift a metal atom away from its equilibrium position in a $2 \times 2 \times 2$ supercell (96 atoms) and calculate and compare the ePDOS of s and d electrons in the metal atoms at the equilibrium and nonequilibrium positions in six pyrite-type dichalcogenides, as shown in Fig. 5. Clearly, for Zn-/Cd-based dichalcogenides, after the metal atoms vibrate away from the equilibrium positions, compared with the electronic orbital energies in the metal atoms at the equilibrium positions, the occupied d -orbital energies move

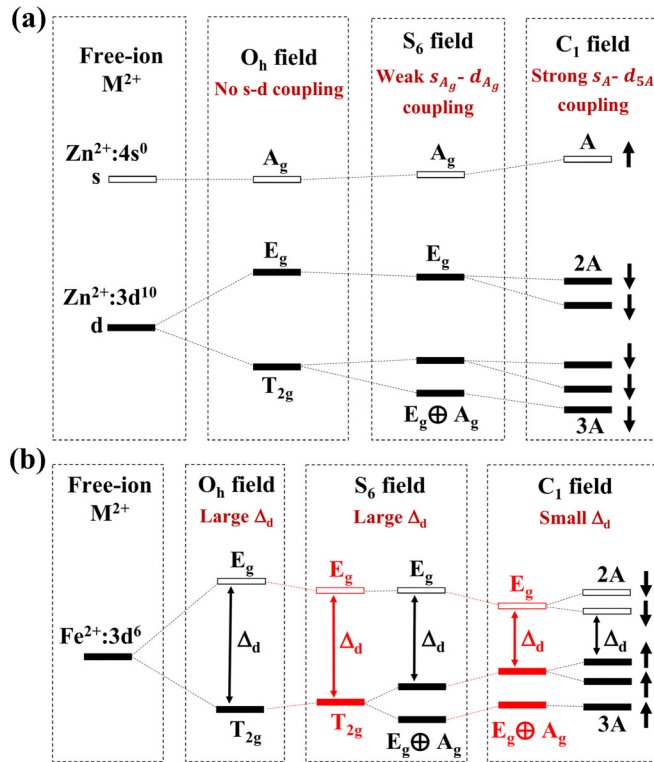


FIG. 4. (a) The crystal field-induced splitting of the d orbitals and the symmetry-controlled s - d coupling effects in metal ions at the +II oxidation state (Zn^{2+}) under different crystal symmetries (from left to right are free-ion, O_h , S_6 , and C_1 field symmetry, respectively). The hollow bars represent unoccupied orbits, and solid bars represent occupied orbits. (b) The electron occupations and crystal splitting energies (Δ_d) of the d orbitals in Fe ions (Fe^{2+}) under different crystal symmetries. The field symmetry decreases from left to right. Note that there is also a reduction of the crystal field splitting Δ_d in (a) when symmetry is reduced, but such a reduction does not affect the total energy because all d orbitals are occupied. The unoccupied $4s$ orbitals in Fe ions (Fe^{2+}) are not shown in (b) for clarity.

down, and the unoccupied s -orbital energy moves up [as shown in Figs. 5(a)/5(b) and 5(d)/5(e)], which exhibits the enhancement of the symmetry-controlled s - d coupling effects between the occupied d orbitals and the unoccupied s orbital. The lowering of the occupied d -orbital energies leads to the decrement of the total energy, thus the slower increase of the potential energy when the metal atoms vibrate away from the equilibrium positions in Zn- and Cd-based dichalcogenides (as shown in Fig. 6), which can result in the soft phonon properties and strong anharmonicities in these systems.

In Fe-based dichalcogenides, when Fe atoms vibrate away from the equilibrium positions, the symmetry-controlled s - d coupling effect is also enhanced between the occupied d electrons and unoccupied s electrons. However, comparing the d -orbital energies in Fe atoms before and after Fe atoms are vibrated, we see the occupied d -orbital energies move up and unoccupied d -orbital energies move down, as shown in Figs. 5(c) and 5(f). This is because, unlike the Zn or Cd atoms where the d orbitals are fully occupied, for Fe

atoms with d^6 configuration, only the T_{2g} -derived states are occupied, whereas the E_g -derived states are empty. Also, because Fe is a transition metal (where the d orbitals are not fully occupied), its d orbitals are relatively delocalized compared with the posttransition metal elements (Zn and Cd). Therefore, the crystal field splitting between the T_{2g} and E_g states (Δ_d) in Fe-based dichalcogenides is larger and more sensitive to the change of the crystal symmetry than that in Zn- and Cd-based dichalcogenides, as shown in Fig. 4(b). When the Fe atom is at the equilibrium position, the site symmetry of the Fe atom is S_6 which is close to O_h , where the d - T_{2g} states are fully occupied and the d - E_g states are not, and the crystal field splitting Δ_d is largest. However, when the Fe atom vibrates away from the equilibrium position, the crystal field splitting Δ_d is decreased due to the reduced symmetry, which will cause the occupied d -orbital energies ($3A$ state derived from T_{2g}) to move up and the unoccupied d -orbital energies ($2A$ state derived from E_g) to move down. As a result, in Fe-based dichalcogenides, when Fe atoms vibrate away from the equilibrium positions, although there is the enhanced s - d coupling effect, due to the weakened crystal field splitting, the occupied d -orbital energies (T_{2g} -derived states) in Fe atoms move up, and the total potential energies rapidly increase (as shown in Fig. 6), which indicates hard phonon properties and weak anharmonicities in Fe-based dichalcogenides. This means that the increment of the energy of the occupied T_{2g} -derived d electrons caused by the weakened crystal field splitting will cancel the symmetry-controlled s - d coupling effect. When the metal atoms are only occupied by T_{2g} -derived d electrons, the cancelling effect is strongest, and with the increase of the occupied E_g -derived d electrons (e.g., in NiS_2 [29]), the cancelling effect will be weaker. Therefore, in Zn- and Cd-based dichalcogenides, since d orbitals in metal atoms are fully occupied, the weakened crystal field splitting has little effect on the total energies of the occupied d orbitals.

To further analyze the anharmonicity, we calculate the total potential energy (V) curves as a function of the displacements (x) of the metal atoms vibrated away from the equilibrium positions along three nonequivalent directions ([100], [110], and [111]) in six different compounds (ZnS_2 , ZnSe_2 , CdS_2 , CdSe_2 , FeS_2 , and FeSe_2), as shown in Fig. S4 in the Supplemental Material [44] and Fig. 6, respectively. By fitting the corresponding quartic anharmonic potential functions $V(x) = Ax^2 + Bx^4$ using the calculated harmonic parameters (A) from the second-order IFC tensors of the metal atoms, the anharmonic parameters (B) are obtained. The calculated parameters (A and B) are listed in Table SI in the Supplemental Material [44]. We find that the calculated values of A in Fe-based dichalcogenides are much larger than those in Zn- and Cd-based dichalcogenides, which indicates that Fe-based dichalcogenides have stronger bonds. The absolute values of B/A calculated along three different directions in all Zn- and Cd-based dichalcogenides are larger than those in Fe-based dichalcogenides, which have the same trend as the calculated maximum Grüneisen parameters (γ_a^{\max} and γ_o^{\max} in Table I). This means that, consistent with the analysis from the changes of ePDOS in Fig. 5, indeed, the vibrations of Zn and Cd atoms exhibit softer phonon properties and stronger anharmonicities than those of Fe atoms. Therefore, we can infer that the

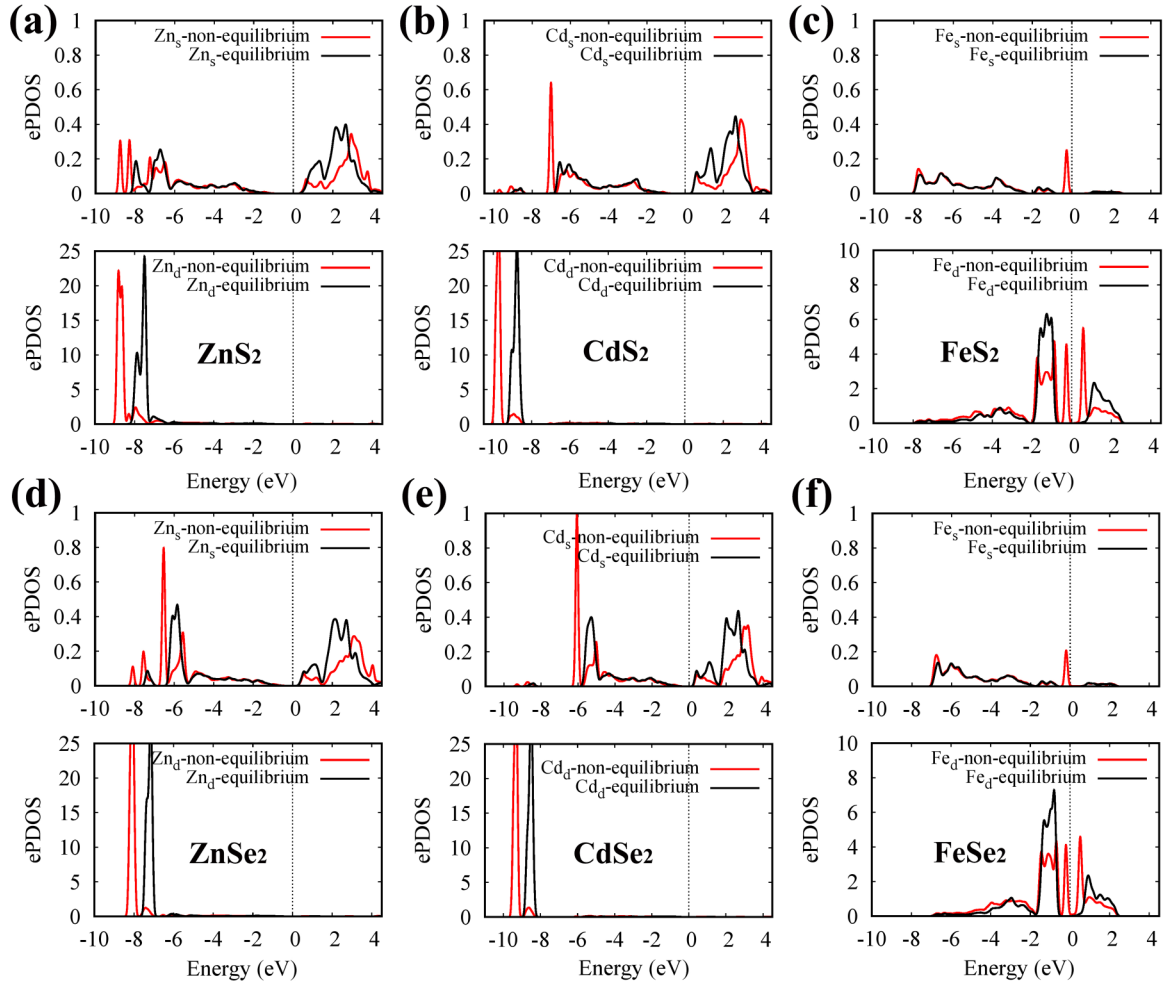


FIG. 5. Calculated electron projected densities of states (ePDOS) of s (up) and d (down) electrons in the metal atoms ($M = \text{Zn}, \text{Cd}$, and Fe) at equilibrium and nonequilibrium positions in (a) ZnS_2 , (b) CdS_2 , (c) FeS_2 , (d) ZnSe_2 , (e) CdSe_2 , and (f) FeSe_2 . The black and red lines represent situations that the metal atoms are located at the equilibrium positions and deviates 5% for Zn/Cd -based dichalcogenides or 3% for Fe -based dichalcogenides from the equilibrium positions along the $[111]$ direction, respectively.

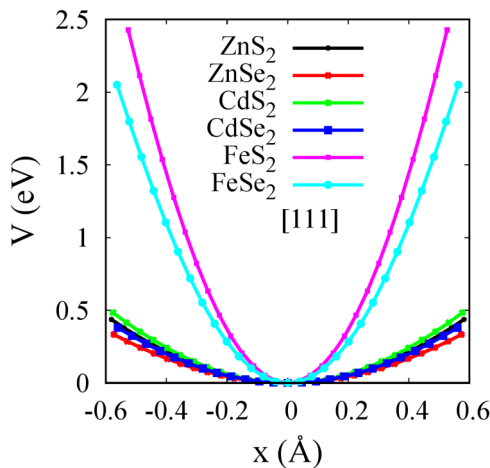


FIG. 6. Calculated total potential energy (V) curves as a function of the displacements (x) of the metal atoms vibrated away from the equilibrium positions along the $[111]$ direction in ZnS_2 , ZnSe_2 , CdS_2 , CdSe_2 , FeS_2 , and FeSe_2 , respectively.

enhanced symmetry-controlled s - d coupling effects and the full occupation of d electrons in metal atoms can synergistically lead to the soft phonon properties and strong anharmonicities in the pyrite-type dichalcogenides.

Furthermore, in the pyrite-type dichalcogenides with the same crystal structure, the strength of the symmetry-controlled s - d coupling effect is decided by the energy difference between the outermost s and d electrons in the metal atoms. To study the influence of the s - d coupling strength on the anharmonicity in different pyrite-type dichalcogenides, we further calculate the anharmonicities in MgS_2 without d electrons and compare them with ZnX_2 and CdX_2 . The calculated energy differences between the outermost s and d electrons (ΔE_{sd}) and maximum Grüneisen parameters in acoustic phonons (γ_a^{\max}) in different pyrite-type dichalcogenides are listed in Table II. From Table II, we can find that the smaller ΔE_{sd} corresponds to the larger γ_a^{\max} , and the calculated γ_a^{\max} in MgS_2 is smallest. This means that a stronger symmetry-controlled s - d coupling effect can contribute to the stronger anharmonicity in pyrite-type dichalcogenides.

TABLE II. Calculated energy differences between the outermost s and d electrons in the metal atoms (ΔE_{sd}) and maximum Grüneisen parameters in acoustic phonons (γ_a^{\max}) in ZnS_2 , ZnSe_2 , CdS_2 , CdSe_2 , and MgS_2 .

MX_2	ZnS_2	ZnSe_2	CdS_2	CdSe_2	MgS_2
ΔE_{sd} (eV)	4.20	4.20	5.93	5.93	–
γ_a^{\max}	4.60	4.60	3.18	2.72	2.07

IV. CONCLUSIONS

In this paper, by comparing the calculated lattice thermal conductivities and phonon properties, we show that the pyrite-type dichalcogenides with similar nonmetallic dimers ($X-X$) and different metal atoms can have very different thermal properties. Compared with Fe-based dichalcogenides, Zn- and Cd-based dichalcogenides have extremely low lattice thermal conductivities, soft phonon modes, and strong

anharmonicities. These unusual behaviors can be explained by the fully occupied and relatively localized d electrons inside the valence bands and the enhanced symmetry-controlled s - d coupling effects in the metal atoms when they vibrate away from the high-symmetry equilibrium positions. On the other hand, for Fe-based pyrite dichalcogenides, because the outermost d electrons in the Fe atom are only occupied by T_{2g} -derived d electrons and more delocalized, the s - d coupling effects are strongly cancelled by the varying crystal field splitting when symmetry is reduced during vibration, so they have higher lattice thermal conductivities. Our work can also be used to explain the origin of the variation in lattice thermal conductivities in other similar metal compounds.

ACKNOWLEDGMENTS

This paper is supported by the National Natural Science Foundation of China, Grants No. 12088101, No. 11991060, No. 12104035, No. 11774347, and No. U2230402, and by the China Postdoctoral Science Foundation, Grant No. 2021M690327.

- [1] H. J. Goldsmid, *Introduction to Thermoelectricity* (Springer, Berlin, Heidelberg, 2016).
- [2] G. A. Slack and S. Galginaitis, *Phys. Rev.* **133**, A253 (1964).
- [3] D. T. Morelli, J. P. Heremans, and G. A. Slack, *Phys. Rev. B* **66**, 195304 (2002).
- [4] Y. Zhang, E. Skoug, J. Cain, V. Ozoliņš, D. Morelli, and C. Wolverton, *Phys. Rev. B* **85**, 054306 (2012).
- [5] G. A. Slack, *Solid State Phys.* **34**, 1 (1979).
- [6] E. S. Toberer, A. Zevalkink, and G. J. Snyder, *J. Mater. Chem.* **21**, 15843 (2011).
- [7] C. Chang, and L.-D. Zhao, *Mater. Today Phys.* **4**, 50 (2018).
- [8] J. Yang, in *Thermal Conductivity: Theory, Properties, and Applications*, edited by T. M. Tritt (Kluwer Academic/Plenum Publishers, New York, 2004), Chap. 1.1, pp. 1–20.
- [9] M. D. Nielsen, V. Ozolins, and J. P. Heremans, *Energy Environ. Sci.* **6**, 570 (2013).
- [10] E. J. Skoug and D. T. Morelli, *Phys. Rev. Lett.* **107**, 235901 (2011).
- [11] S. Lee, K. Esfarjani, T. Luo, J. Zhou, Z. Tian, and G. Chen, *Nat. Commun.* **5**, 3525 (2014).
- [12] M. Christensen, A. B. Abrahamsen, N. B. Christensen, F. Juranyi, N. H. Andersen, K. Lefmann, J. Andreasson, C. R. H. Bahl, and B. B. Iversen, *Nat. Mater.* **7**, 811 (2008).
- [13] Z. Feng, T. Jia, J. Zhang, Y. Wang, and Y. Zhang, *Phys. Rev. B* **96**, 235205 (2017).
- [14] M. K. Jana, K. Pal, A. Warankar, P. Mandal, U. V. Waghmare, and K. Biswas, *J. Am. Chem. Soc.* **139**, 4350 (2017).
- [15] W. Schweika, R. P. Hermann, M. Prager, J. Perßon, and V. Keppens, *Phys. Rev. Lett.* **99**, 125501 (2007).
- [16] T. Jia, J. Carrete, Z. Feng, S. Guo, Y. Zhang, and G. K. H. Madsen, *Phys. Rev. B* **102**, 125204 (2020).
- [17] T. Jia, J. Carrete, G. K. H. Madsen, Y. Zhang, and S.-H. Wei, *Phys. Rev. B* **105**, 245203 (2022).
- [18] W. G. Zeier, A. Zevalkink, Z. M. Gibbs, G. Hautier, M. G. Kanatzidis, and G. J. Snyder, *Angew. Chemie Int. Ed.* **55**, 6826 (2016).
- [19] J. Ma and S.-H. Wei, *Phys. Rev. Lett.* **110**, 235901 (2013).
- [20] H.-X. Deng, J.-W. Luo, S.-S. Li, and S.-H. Wei, *Phys. Rev. Lett.* **117**, 165901 (2016).
- [21] Z.-H. Wang, X. Zhang, and S.-H. Wei, *J. Phys. Chem. Lett.* **13**, 11438 (2022).
- [22] K. Yang, H. Yang, Y. Sun, Z. Wei, J. Zhang, J.-W. Luo, P.-H. Tan, S.-S. Li, S.-H. Wei, and H.-X. Deng, *arXiv:2102.12619*.
- [23] T. A. Bither, R. J. Bouchard, W. H. Cloud, P. C. Donohue, and W. J. Siemons, *Inorg. Chem.* **7**, 2208 (1968).
- [24] K. Kato, Y. Okamoto, J. Morimoto, and T. Miyakawa, *J. Mater. Sci. Lett.* **16**, 914 (1997).
- [25] V. K. Gudelli, V. Kanchana, S. Appalakondaiah, G. Vaitheeswaran, and M. C. Valsakumar, *J. Phys. Chem. C* **117**, 21120 (2013).
- [26] V. K. Gudelli, V. Kanchana, G. Vaitheeswaran, M. C. Valsakumar, and S. D. Mahanti, *RSC Adv.* **4**, 9424 (2014).
- [27] Y. Xu, W. Li, C. Wang, Z. Chen, Y. Wu, X. Zhang, J. Li, S. Lin, Y. Chen, and Y. Pei, *J. Materiomics* **4**, 215 (2018).
- [28] K. Wang, A. Wang, A. Tomic, L. Wang, A. M. M. Abeykoon, E. Dooryhee, S. J. L. Billinge, and C. Petrovic, *APL Mater.* **3**, 041513 (2015).
- [29] A. Maignan, R. Daou, E. Guilmeau, D. Berthebaud, T. Barbier, O. Lebedev, and S. Hébert, *Phys. Rev. Mater.* **3**, 115401 (2019).
- [30] P. A. Popov, P. P. Fedorov, and S. V. Kuznetsov, *Cryst. Rep.* **58**, 319 (2013).
- [31] S. Hébert, E. Guilmeau, D. Berthebaud, O. I. Lebedev, V. Roddatis, and A. Maignan, *J. Appl. Phys.* **114**, 103703 (2013).
- [32] T. Jia, Z. Feng, S. Guo, X. Zhang, and Y. Zhang, *ACS Appl. Mater. Interfaces* **12**, 11852 (2020).
- [33] G. Kresse and J. Furthmüller, *Phys. Rev. B* **54**, 11169 (1996).
- [34] G. Kresse and D. Joubert, *Phys. Rev. B* **59**, 1758 (1999).
- [35] J. P. Perdew, K. Burke, and M. Ernzerhof, *Phys. Rev. Lett.* **77**, 3865 (1996).
- [36] V. I. Anisimov, J. Zaanen, and O. K. Andersen, *Phys. Rev. B* **44**, 943 (1991).

- [37] J. Hu, Y. Zhang, M. Law, and R. Wu, *Phys. Rev. B* **85**, 085203 (2012).
- [38] H. J. Monkhorst and J. D. Pack, *Phys. Rev. B* **13**, 5188 (1976).
- [39] R. Sun, M. K. Y. Chan, and G. Ceder, *Phys. Rev. B* **83**, 235311 (2011).
- [40] J. Heyd, G. E. Scuseria, and M. Ernzerhof, *J. Chem. Phys.* **118**, 8207 (2003).
- [41] A. V. Krukau, O. A. Vydrov, A. F. Izmaylov, and G. E. Scuseria, *J. Chem. Phys.* **125**, 224106 (2006).
- [42] P. Borlido, J. Schmidt, A. W. Huran, F. Tran, M. A. L. Marques, and S. Botti, *npj Comput. Mater.* **6**, 96 (2020).
- [43] A. Alkauskas, P. Broqvist, and A. Pasquarello, *Phys. Rev. Lett.* **101**, 046405 (2008).
- [44] See Supplemental Material at <https://link.aps.org/supplemental/10.1103/PhysRevB.107.115204> for the calculated electronic band structures and the total potential energy curves as a function of the displacements of the metal atoms vibrated away from the equilibrium positions along the [111] direction in three pyrite-type dichalcogenides (ZnS_2 , CdS_2 , and FeS_2) using the different computational methods (PBE, PBE+ U under different U values, and HSE); the calculated total potential energy curves as a function of the displacements of the metal atoms vibrated away from the equilibrium positions along the [100] and [110] directions, and the calculated parameters (A and B) by fitting the quartic anharmonic potential functions $V(x) = Ax^2 + Bx^4$, when the metal atoms vibrate away from the equilibrium positions along the [100], [110], and [111] directions in ZnS_2 , ZnSe_2 , CdS_2 , CdSe_2 , FeS_2 , and FeSe_2 , respectively.
- [45] A. Togo, F. Oba, and I. Tanaka, *Phys. Rev. B* **78**, 134106 (2008).
- [46] J. Carrete, B. Vermeersch, A. Katre, A. van Roekeghem, T. Wang, G. K. H. Madsen, and N. Mingo, *Comput. Phys. Commun.* **220**, 351 (2017).
- [47] W. Li, J. Carrete, N. A. Katcho, and N. Mingo, *Comput. Phys. Commun.* **185**, 1747 (2014).